arXiv:cond-mat/0105370v1 [cond-mat.supr-con] 18 May 2001

The London theory of the crossing-vortex lattice in highly anisotropic layered superconductors

S.E. Savel'ev*, J. Mirković+, and K. Kadowaki
Institute of Materials Science, The University of Tsukuba, 1-1-1 Tennodai, Tsukuba 305-8573, Japan, and
CREST, Japan Science and Technology Corporation (JST), Japan

A novel description of Josephson vortices (JVs) crossed by the pancake vortices (PVs) is proposed on the basis of the anisotropic London equations. The field distribution of a JV and its energy have been calculated for both dense ($a < \lambda_J$) and dilute ($a > \lambda_J$) PV lattices with distance a between PVs, and the nonlinear JV core size λ_J. It is shown that the "shifted" PV lattice (PVs displaced mainly along JVs in the crossing vortex lattice structure), formed in high out-of-plane magnetic fields $B_z > \Phi_0/\gamma^2 s^2$ [A.E. Koshelev, Phys. Rev. Lett. **83**, 187 (1999)], transforms into the PV lattice "trapped" by the JV sublattice at a certain field, lower than $\Phi_0/\gamma^2 s^2$, where Φ_0 is the flux quantum, γ is the anisotropy parameter and s is the distance between CuO$_2$ planes. With further decreasing B_z, the free energy of the crossing vortex lattice structure (PV and JV sublattices coexist separately) can exceed the free energy of the tilted lattice (common PV-JV vortex structure) in the case of $\gamma s < \lambda_{ab}$ with the in-plane penetration depth λ_{ab} if the low ($B_x < \gamma\Phi_0/\lambda_{ab}^2$) or high ($B_x \gtrsim \Phi_0/\gamma s^2$) in-plane magnetic field is applied. It means that the crossing vortex structure is realized in the intermediate field orientations, while the tilted vortex lattice can exist if the magnetic field is aligned near the c-axis and the ab-plane as well. In the intermediate in-plane fields $\gamma\Phi_0/\lambda_{ab}^2 \lesssim B_x \lesssim \Phi_0/\gamma s^2$, the crossing vortex structure with the "trapped" PV sublattice seems to settle in until the lock-in transition occurs since this structure has the lower energy with respect to the tilted vortex structure in the magnetic field **H** oriented near the ab-plane. The recent experimental results concerning the vortex lattice melting transition and transitions in the vortex solid phase in Bi$_2$Sr$_2$CaCu$_2$O$_{8+\delta}$ single crystals are discussed in the context of the presented theoretical model.

PACS numbers: 74.60.Ge, 74.60.Ec, 74.72.Hs

The mixed state of high temperature superconductors is complex and rich with various vortex phases[1,2]. Besides the vortex lattice described by 3D anisotropic Ginzburg-Landau model, the new types of vortex structures can occur within the large part of the phase diagram of the mixed state where the coherence length along the c-axis is smaller than the distance between CuO$_2$ planes. In such a case, the magnetic field, aligned with the c-axis, penetrates a superconductor in the form of quasi two-dimensional pancake vortices (PVs)[3] while the field applied parallel to the ab-plane generates Josephson vortices (JVs) in the layers between CuO$_2$ planes[4,5]. In magnetic fields tilted with respect to the c-axis, PVs and JVs can form a common tilted lattice[5] or exist separately as a crossing (combined) lattice[6,7]. The tilted lattice represents the inclined PVs stacks in fields applied close to the c-axis while, at higher angles, the pieces of JVs linking PVs are developed[5,6]. The crossing lattice is another structure containing both a PV stack sublattice and a JV sublattice which coexist separately.

The vortex-solid phase diagram in the tilted magnetic fields was first proposed by Bulaevskii, Ledvij, and Kogan[6]. According to their model, which does not take into account the interaction between PV and JV sublattices in the crossing lattice structure, the tilted lattice is formed for all orientations of the magnetic field until the lock-in transition[8] occurs if the in-plane London penetration depth λ_{ab} is larger than the Josephson vortex core with size γs (γ is the anisotropy parameter and s is the distance between CuO$_2$ planes). In the opposite limit, $\gamma s > \lambda_{ab}$, the tilted lattice transforms into the crossing lattice (as the magnetic field is inclined away from the c-axis) at a certain angle before the lock-in transition happens[6]. Later, the possibility of the coexistence of two vortex sublattices with different orientations was analyzed numerically by comparing the free energy of such system with the free energy of mono-oriented tilted vortex lattice at different field orientations and different absolute values of the external magnetic field for the case of 3D anisotropic (London model) superconductors[9–11] as well as layered (Lawrence-Doniach model[12]) superconductors[13]. According to that analysis[11,13] performed for $\gamma = 50 - 160$, the crossing lattice can be energetically preferable in the quite low magnetic fields ($B = \sqrt{B_z^2 + B_x^2} \lesssim \Phi_0/\lambda_{ab}^2$) in the intermediate field orientations $0 < \theta_1 < \theta < \theta_2 < \pi/2$ with $\theta = \arctan(B_x/B_z)$ (B_z and B_x are the field component along the c-axis and parallel to the ab-plane, respectively). However, the interaction of two coexisting vortex sublattices was not considered in those works[9–11,13]. Recently, Koshelev[7] has studied the case of extremely anisotropic superconductors $\gamma s \gg \lambda_{ab}$ and has shown that the crossing lattice can occupy substantially larger region of the vortex lattice phase diagram in the oblique fields due to the renormalization of the JV energy $\mathcal{E}_J$ through the interaction of a Josephson vortex and the PV sublattice. In addition, such interaction leads to the attraction of PVs to JVs[14,7] at low out-of-plane magnetic fields B_z

(the some sort of pinning effect). This pinning may induce transitions between different substructures of the crossing lattice structure. However, there is still no theoretical investigation how PV sublattice can influence on the JV lattice in the crossing vortex structure in the case of moderate anisotropic superconductors with $\gamma s < \lambda_{ab}$. In this regard, the phase diagram[6] of the vortex lattice for strongly anisotropic layered superconductors should be reconsidered (at least for the case of $\gamma s < \lambda_{ab}$) by taking into account the renormalization of $\mathcal{E}_J$ and the pinning of PVs by JVs.

The vortex structures in highly anisotropic layered superconductors are usually studied on the basis of the nonlinear discrete Lawrence-Doniach model[12], but this model is quite complex and the detailed analysis of the vortex system is complicated. On the other hand, the layerness of superconductors can be ignored on scales larger than the size of the nonlinear Josephson vortex core. Therefore, the linear anisotropic London model could be applied for a study of the vortex crossing lattice outside JV cores. In this paper we introduce the extended London theory which allows to describe the crossing lattice as well as to calculate the energy $\mathcal{E}_J$ and the field distribution of JV in the presence of the crossed PV sublattice. It is shown that with decreasing the perpendicular magnetic field the pancake sublattice transforms from the "shifted" sublattice characterized by one component PV displacement along JVs to the "trapped" sublattice where JVs are occupied by PV rows. The comparison of the free energies of the tilted lattice and the crossing vortex structure for the case $\lambda_{ab} > \gamma s$ indicates that in low ($B_x \lesssim \gamma\Phi_0/\lambda_{ab}^2$) and high ($B_x \gtrsim \Phi_0/\gamma s^2$) in-plane fields, the tilted lattice can exist if the vector $\mathbf{B} = B_x\mathbf{e}_x + B_z\mathbf{e}_z$ is directed close to the c-axis as well as near the ab-plane, while the crossing lattice is realized in the fields oriented far enough from the crystal symmetry axes. Furthermore, in the intermediate in-plane fields the tilted vortex lattice exists only at the magnetic field orientations near the c-axis whereas crossing vortex structure settles in the wide angular range until the lock-in transition happens.

This paper is organized as follows. The general equations for the magnetic field distribution and the energy of Josephson vortex in the presence of the pancake lattice are derived in section I. The dense pancake lattice is studied in section II. It is shown that, in the limit $\gamma s \gg \lambda_{ab}$ and $\Phi_0/(\gamma s)^2 \ll B_z \ll \Phi_0\gamma^2 s^2/\lambda_{ab}^4$, our model reproduces the results which were earlier obtained by Koshelev[7], while the shear deformation of the PV lattice significantly renormalizes the JV energy at the higher out-of-plane fields. Section III is devoted to the dilute PV lattice. It is described how the novel vortex substructure with the PV lattice "trapped" by the JV lattice can be realized at low B_z. The phase diagram of the vortex-solid phase in the tilted magnetic fields is considered for the case of $\lambda_{ab} > \gamma s$ in section IV while the recent experimental results are discussed in section V.

I. JOSEPHSON VORTEX IN THE PRESENCE OF PANCAKE VORTEX LATTICE: GENERAL EQUATIONS

We consider a Josephson vortex crossed with the pancake lattice in the framework of the modified London model. On scales which are much larger than both the distance between CuO$_2$ planes and the in-plane coherence length ξ_{ab}, the pancake vortex stack could be considered as an ordinary vortex line at temperatures significantly lower than the evaporation temperature[3,15]. The same approach can be also used for the description of the Josephson vortex far from the nonlinear core. The JV current acts on PVs through the Lorentz force causing their displacements along JV, which can be interpreted as a local inclination of the PV lines away from the c-axis. In turn, the local tilt of the PV stacks induces an additional current along the c-axis which redistributes the "bare" JV field. Such physical picture can be described with one-component PV displacement $\mathbf{u} = (u, 0, 0)$ which does not depend on the x-coordinate (Fig. 1). The free energy functional $\mathcal{F}_{PJ}$ can be written as

$$\mathcal{F}_{PJ} = \frac{1}{8\pi}\int d^3\mathbf{R}\Big(\mathbf{h}_p^2 + \nabla\times\mathbf{h}_p\overset{\leftrightarrow}{\Lambda}\nabla\times\mathbf{h}_p + \mathbf{h}_J{}^2 + \nabla\times\mathbf{h}_J\overset{\leftrightarrow}{\Lambda}\nabla\times\mathbf{h}_J + 2\mathbf{h}_p\mathbf{h}_J + 2\nabla\times\mathbf{h}_p\overset{\leftrightarrow}{\Lambda}\nabla\times\mathbf{h}_J\Big), \tag{1}$$

where $\mathbf{h}_p$ and $\mathbf{h}_J$ are the magnetic fields of PV lines and JV, respectively, and $\overset{\leftrightarrow}{\Lambda}$ is the penetration-depth tensor, $\nabla = (\partial/\partial x, \partial/\partial y, \partial/\partial z)$. In the considered coordinate system the tensor has only the diagonal components $\Lambda_{xx} = \Lambda_{yy} = \lambda_{ab}^2$, $\Lambda_{zz} = \lambda_c^2$ with anisotropic penetration depths λ_{ab} and λ_c. The field $\mathbf{h}_p$ is determined by the displacement u of PVs through the London equation (see, for instance,[2])

$$\mathbf{h}_p + \nabla\times\left(\overset{\leftrightarrow}{\Lambda}\nabla\times\mathbf{h}_p\right) = \Phi_0\sum_i\int d\tilde{z} \times\left(\mathbf{e}_z + \frac{\partial u(Y_i,\tilde{z})\mathbf{e}_x}{\partial\tilde{z}}\right)\delta(\mathbf{r} - \mathbf{R}_i(\tilde{z}) - u(Y_i,\tilde{z})\mathbf{e}_x), \tag{2}$$

where $\mathbf{R}_i(\tilde{z}) = (X_i, Y_i, \tilde{z})$ is the equilibrium position of the i-th PV line, $\mathbf{r} = (x, y, z)$ while $\mathbf{e}_z$ and $\mathbf{e}_x$ are unit vectors along the z and x axes, respectively. (Here we have accepted that the parametric equation $\mathbf{r}_i(\tilde{z})$ (with parameter $\tilde{z}$) describing the i-th vortex line takes the form of $x(\tilde{z}) = X_i + u_i(\tilde{z})$, $y(\tilde{z}) = Y_i$, $z(\tilde{z}) = z$.) The in-plane coordinates of the unshifted lines X_i and Y_i are expressed through the distances a and b (see Fig. 1 b) between PVs and PV rows as $X_i = al/2 + aj$ and $Y_i = bl$ with integer l and j. In our approach, the field of the Josephson vortex also obeys the London equation

$$h_J - \lambda_{ab}^2\frac{\partial^2 h_J}{\partial z^2} - \lambda_c^2\frac{\partial^2 h_J}{\partial y^2} = \Phi_0\delta(y)\delta(z), \tag{3}$$

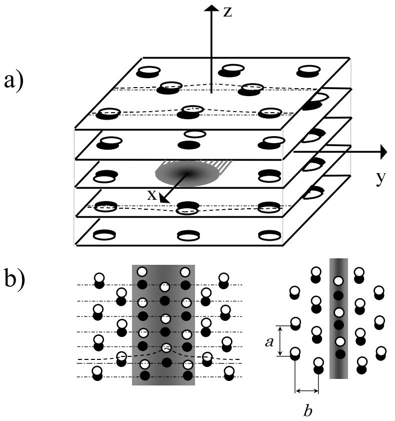

FIG. 1. The JV crossed by PV stacks which are shifted by the currents induced by JV: a) 3D sketch depicts the deformation of the PV lattice in the different CuO$_2$ planes, b) 2D sketches show the deformation of the PV lattice in a CuO$_2$ plane for the dense (left) and dilute (right) PV lattices. The filled circles correspond to the unshifted PVs while the open ones represent the PVs shifted due to the interaction with JV currents. The shaded area images the nonlinear JV core region. The dashed-dotted lines mark the rows of the unshifted PVs while the dashed curve shows the deviation of PVs from these rows.

where δ-functions should be smoothed on a scale of the Josephson vortex core. The JV core size along the z-axis is fixed by the interlayer distance s, while the core length along the y-direction is limited by the condition that the current along the c-axis can not exceed the maximum interlayer current $j_c \sim c\Phi_0/(8\pi^2\lambda_c^2 s)$. In the presence of PVs, the current across the layers consists of both the current of JV itself and the current born by the local inclination of PV lines. Therefore, the core size along the y-axis λ_J can be renormalized in the presence of PVs and should be calculated self-consistently (see next section). Furthermore, the space variable y could be replaced by $y - y_0$ in the argument of the δ-function with $0 \leq y_0 \leq b$ since the PV lattice can be arbitrary shifted from the center of JV. However, we take $y_0 = 0$ which corresponds to the energetically more preferable position[7].

Next, in order to find the distribution of the magnetic field in the vortex system and the energy of JV, we will minimize the free energy (1) as a functional of the displacement u. The fields $\mathbf{h}_p$ and $\mathbf{h}_J$ can be obtained using equations (2,3) with the displacement u fixed by the minimization of (1). Then, the energy of JV, $\mathcal{E}_J$, defined as the difference of the free energies (1) with and without JV, will be derived. This energy includes the self energy of JV and the change of the free energy of the PV lattice born by the interaction with JV. We will use the elastic approximation, *i.e.*, the free energy (1) and the magnetic field of PVs (2) will be expanded up to the second order in u.

Using the integral representation of δ-function, the equation (2) can be rewritten as

$$\mathbf{h}_p+\nabla\times\left(\overset{\leftrightarrow}{\Lambda}\nabla\times\mathbf{h}_p\right)=\Phi_0\sum_i\int d\tilde{z}$$

$$\times\int\frac{d^3\mathbf{q}}{(2\pi)^3}e^{i\mathbf{qr}}e^{-i\mathbf{q}\mathbf{R}_i(\tilde{z})}\Bigg(\mathbf{e}_z(1-iq_xu_i(\tilde{z})-\frac{1}{2}q_x^2u_i^2(\tilde{z}))$$

$$+\frac{\partial u_i(\tilde{z})}{\partial\tilde{z}}(1-iq_xu_i(\tilde{z}))\mathbf{e}_x\Bigg). \qquad (4)$$

The field $\mathbf{h}_p$ of PV lines changes on different space scales. The first scale is determined by the characteristic gradient of the displacement $u(y,z)$ and usually is much larger than the distance a between PVs. The second scale is defined by the discreteness of the PV lattice and it is about a. To separate the contribution to the free energy from these scales, we introduce the Fourier variables $u(k_y,k_z)$:

$$u(Y_i,z)=\int_{-\pi/b}^{\pi/b}\frac{dk_y}{2\pi}\int\frac{dk_z}{2\pi}u(k_y,k_z)e^{i(k_yY_i+k_zz)}, \qquad (5)$$

and

$$u(k_y,k_z)=b\sum_{Y_i}\int dz u(Y_i,z)e^{-i(k_yY_i+k_zz)}, \qquad (6)$$

where the domain of variation of k_z is restricted by the inequality $|k_z| \lesssim 1/s$ born by the layerness of the system. Substituting (5) into (4) and using the well-known equality $\sum_i\int d\tilde{z}\exp\left(i(\mathbf{k}-\mathbf{q})\mathbf{R}_i(\tilde{z})\right) = (2\pi)^3(B_z/\Phi_0)\sum_{\mathbf{Q}}\delta(\mathbf{k}-\mathbf{q}-\mathbf{Q})$, where $\mathbf{Q}=(Q_x,Q_y,0)$ are the vectors of the reciprocal lattice ($Q_x = 2\pi m/a, Q_y=\pi(2n+m)/b$ with integer m and n), one gets the expansion of the field of PVs in series with respect to the displacement u:

$$\mathbf{h}_p=\mathbf{h}_p^{(0)}+\mathbf{h}_p^{(1)}[u]+\mathbf{h}_p^{(2)}[u], \quad \mathbf{n}_p=\mathbf{n}_p^{(0)}+\mathbf{n}_p^{(1)}[u]+\mathbf{n}_p^{(2)}[u],$$

$$\mathbf{h}_p^{(i)}+\nabla\times\overset{\leftrightarrow}{\Lambda}\nabla\times\mathbf{h}_p^{(i)}=\mathbf{n}_p^{(i)} \qquad (7)$$

where

$$\mathbf{n}_p^{(0)}=\mathbf{e}_z\Phi_0\sum_i\delta_2(\mathbf{r}^\perp-\mathbf{R}_i^\perp),$$

$$\mathbf{n}_p^{(1)}=B_z\sum_{\mathbf{Q}}\int\frac{dk_ydk_z}{4\pi^2}$$

$$\times(\mathbf{e}_ziQ_x+\mathbf{e}_xik_z)u(k_y,k_z)e^{-iQ_xx}e^{i(k_y-Q_y)y}e^{ik_zz},$$

$$\mathbf{n}_p^{(2)}=B_z\sum_{\mathbf{Q}}\int\frac{dk_ydk_zdk'_ydk'_z}{16\pi^4}u(\mathbf{k})u(\mathbf{k}')$$

$$\times\left(-\frac{1}{2}Q_x^2\mathbf{e}_z-Q_xk_z\mathbf{e}_x\right)e^{i(k_z+k'_z)z}e^{-iQ_xx}e^{i(k_y+k'_y-Q_y)y}. \qquad (8)$$

The term of $\mathbf{h}_p$ with $\mathbf{Q} = 0$ corresponds to the continuous approximation and varies on the large scale, while terms with $\mathbf{Q} \neq 0$ are related to the field components changing on the scale of a.

It is easy to see that only terms with $Q_x = 0$ will give contribution to the part of the free energy describing the interaction between PVs and JV, because the field $\mathbf{h}_J$ does not depend on x and all terms with $Q_x \neq 0$ vanish after integration over x. Therefore, it is convenient to divide $\mathbf{h}_p^{(1)}$ and $\mathbf{n}_p^{(1)}$ into two components: $\mathbf{n}_p^{(1)} = \mathbf{n}_p^{(Q)} + \mathbf{e}_x n_p^*$, $\mathbf{h}_p^{(1)} = \mathbf{h}_p^{(Q)} + \mathbf{e}_x h_p^*$, where $\mathbf{h}_p^{(Q)}$ and $\mathbf{n}_p^{(Q)}$ include summands with $Q_x \neq 0$ while h_p^* and n_p^* do not vary with x. Then, the free energy functional F_{cross}, containing only terms dependent on the displacement u, can be introduced as $F_{cross} = \mathcal{F}_{PJ} - \mathcal{F}_P - \mathcal{F}_J$, where $\mathcal{F}_P$ and $\mathcal{F}_J$ are the free energies of the unperturbed PV lattice and the "bare" JV, respectively. Using equations (7), we obtain the expression for F_{cross} as

$$F_{cross} = \frac{1}{8\pi} \int d^3\mathbf{R} \left(\mathbf{n}_p^{(Q)} \mathbf{h}_p^{(Q)} + 2\mathbf{h}_p^{(0)} \mathbf{n}_p^{(2)} \right) + \frac{1}{8\pi} \int d^3\mathbf{R} \left(h_p^* n_p^* + 2 h_J n_p^* \right). \quad (9)$$

The first contribution comes from the terms with $Q_x \neq 0$ and depends only on the short-scale variations of $\mathbf{h_p}$. It is determined by the shear deformation and the tilt deformation. The second part describes the interaction of PVs with JV and with the current generated by PVs along the y-axis. Using the equations (8), the free energy F_{cross} can be rewritten in term of Fourier variables $u(k_y, k_z)$:

$$F_{cross} = \frac{1}{2} \int \frac{dk_y dk_z}{4\pi^2} \left(U_{66}(k_y) + U_{44}(k_y, k_z) \right) u(\mathbf{k}) u(-\mathbf{k}) + \frac{B_z \Phi_0}{4\pi} \sum_{Q_x=0} \int \frac{dk_y dk_z}{4\pi^2} i k_z u(\mathbf{k}) \times \frac{f(k_z, k_y - Q_y) - (B_z/2\Phi_0) i k_z u(-\mathbf{k})}{1 + \lambda_{ab}^2 k_z^2 + \lambda_c^2 (k_y - Q_y)^2}, \quad (10)$$

with the shear energy

$$U_{66} = \frac{B_z^2}{4\pi} \sum_{Q_x \neq 0} \left\{ \frac{Q_x^2}{1 + \lambda_{ab}^2 Q_x^2 + \lambda_{ab}^2 (k_y - Q_y)^2)} - \frac{Q_x^2}{1 + \lambda_{ab}^2 (Q_x^2 + Q_y^2)} \right\}, \quad (11)$$

and the tilt energy

$$U_{44} = \frac{B_z^2}{4\pi} \sum_{Q_x \neq 0} \left\{ \frac{Q_x^2}{1 + \lambda_{ab}^2 k_z^2 + \lambda_{ab}^2 Q_x^2 + \lambda_{ab}^2 (k_y - Q_y)^2} - \frac{Q_x^2}{1 + \lambda_{ab}^2 Q_x^2 + \lambda_{ab}^2 (Q_y - k_y)^2} + \frac{k_z^2}{1 + \lambda_{ab}^2 k_z^2 + \lambda_c^2 Q_x^2 + \lambda_c^2 (k_y - Q_y)^2} + \frac{(\lambda_c^2 - \lambda_{ab}^2) Q_x^2 k_z^2}{(1 + \lambda_{ab}^2 k_z^2 + \lambda_{ab}^2 Q_x^2 + \lambda_{ab}^2 (k_y - Q_y)^2)} \times \frac{1}{(1 + \lambda_c^2 Q_x^2 + \lambda_c^2 (k_y - Q_y)^2 + \lambda_{ab}^2 k_z^2)} \right\}. \quad (12)$$

The expressions for U_{44} and U_{66} represent sums over the reciprocal lattice vectors with $Q_x \neq 0$, while the summation in the last term of (10) is performed only over the reciprocal lattice vectors with $Q_x = 0$. The function $f(\mathbf{q})$ in (10) appears due to smoothing of δ function in eq. (3) and can be evaluated as $f(\mathbf{q}) \approx 1$ in the rectangular region $|q_z| \leq 1/s$, $|q_y| \leq 1/\lambda_J$ and $f \approx 0$ outside that area. The summation in the expression (11) for the shear elastic energy was done by Brandt[16] in the limit $k_y \ll \pi/b$:

$$U_{66} = C_{66} k_y^2, \quad (13)$$

where the shear elastic modulus C_{66} is expressed as $C_{66} = (B_z \Phi_0)/(8\pi\lambda_{ab})^2$ for $a_0 = \sqrt{\Phi_0/B_z} < \lambda_{ab}$, while $C_{66} = \sqrt{\pi\lambda_{ab}/(6a_0)} \Phi_0^2/(4\pi\lambda_{ab}^2)^2 \exp(-a_0/\lambda_{ab})$ for $a_0 > \lambda_{ab}$. The tilt energy was obtained in[2,17]:

$$U_{44} = \frac{B_z \Phi_0}{32\pi^2 \lambda_{ab}^4} \left(\ln\left(1 + \frac{k_z^2}{\lambda_{ab}^{-2} + K_0^2} \right) + \frac{k_z^2 \lambda_{ab}^4}{\lambda_c^2} \ln\left(\frac{\xi_{ab}^{-2}}{K_0^2 + (k_z^2/\gamma^2) + \lambda_c^{-2}} \right) \right) \quad (14)$$

for $k_z \gtrsim K_0 = 2\pi/b$, while

$$U_{44} = \left(3.68 \frac{\Phi_0^2}{(4\pi\lambda_{ab})^4} + \frac{B_z \Phi_0 \ln(a^2/\xi_{ab}^2)}{32\pi^2 \lambda_c^2} \right) k_z^2 = C_{44}^{eff} k_z^2 \quad (15)$$

for $k_z \ll K_0$. Performing summation over Q_y in the second term of equation (10) (see Appendix A), we finally obtain the free energy functional:

$$F_{cross} = \int \frac{dk_y}{2\pi} \frac{dk_z}{2\pi} \left\{ \frac{1}{2} \left(U_{44} + U_{66} \right) u(\mathbf{k}) u(-\mathbf{k}) + \frac{B_z}{4\pi} i k_z \Psi(k_z, k_y) \left(u(\mathbf{k}) - i k_z \frac{B_z}{2\Phi_0} u(\mathbf{k}) u(-\mathbf{k}) \right) \right\}, \quad (16)$$

where Ψ is defined by the equation

$$\Psi(k_z, k_y) = \frac{\Phi_0 b}{2\lambda_c \sqrt{1 + \lambda_{ab}^2 k_z^2}} \times \frac{\sinh\left(\sqrt{1 + \lambda_{ab}^2 k_z^2}\, b/\lambda_c \right)}{\cosh\left(\sqrt{1 + \lambda_{ab}^2 k_z^2}\, b/\lambda_c \right) - \cos k_y b} \quad (17)$$

for $k_y < \min(\pi/b,\ 1/\lambda_J)$ and $k_z < 1/s$ while $\Psi \approx 0$ outside that rectangular area. In the case of small values of wave vector $\mathbf{k}$ ($k_y \ll \pi/b$ and $k_z \ll \gamma/b$), the discreteness of PV lattice is irrelevant and the function Ψ coincides with the Fourrier image of the "bare" JV field, but Ψ is modified substantially for larger k_y or k_z.

The minimization of the free energy functional (16) determines the displacement u as

$$u(\mathbf{k}) = \frac{B_z}{4\pi}\frac{ik_z\Psi(\mathbf{k})}{U_{44}+U_{66}+(B_z^2k_z^2/4\pi\Phi_0)\Psi(\mathbf{k})}. \tag{18}$$

In order to describe the field distribution of a JV in the crossing lattice, the averaged magnetic induction $\mathcal{B}_J$ along the x-direction generated by both JV and inclined PV lines can be introduced. By substituting the found displacement (18) into equations (7,8), the magnetic induction of JV $\mathcal{B}_J = h_J + h_p^*$ is rewritten as

$$\mathcal{B}_J = \int\frac{dq_zdq_y}{(2\pi)^2}\frac{\Phi_0e^{iq_yy+iq_zz}}{1+\lambda_c^2q_y^2+\lambda_{ab}^2q_z^2} + B_z\sum_{Q_y}\int\frac{dk_ydk_z}{(2\pi)^2}\frac{ik_zu(\mathbf{k})}{1+\lambda_c^2(k_y-Q_y)^2+k_z^2\lambda_{ab}^2}e^{i(k_y-Q_y)+ik_zz}, \tag{19}$$

where q_y and q_z are the wave vectors of a "bare" JV ($|q_y| < 1/\lambda_J$, $|q_z| < 1/s$), while the wave vectors $\mathbf{k}$ of the PV lattice are restricted also by the first Brillouin zone of the PV lattice ($|k_y| < \min(1/\lambda_J,\ \pi/b)$, $|k_z| < 1/s$). To get the energy $\mathcal{E}_J$ it is necessary to add F_{cross} to the energy of the JV itself. Obviously, the energy of a JV in the presence of PV lines is always lower than one of a "bare" JV. Indeed, for the displacement of PVs u determined by equation (18), the energy F_{cross} takes the minimum value which is smaller than zero, since $F_{cross} = 0$ at $u = 0$. Finally, the energy of JV in the crossing lattice obeys the equation

$$\mathcal{E}_J = \frac{\Phi_0^2}{8\pi}\int\frac{dq_ydq_z}{(2\pi)^2}\frac{1}{1+\lambda_c^2q_y^2+\lambda_{ab}^2q_z^2} - \frac{B_z^2}{32\pi^2}\int\frac{dk_ydk_z}{(2\pi)^2}\frac{k_z^2\Psi(\mathbf{k})\Psi(-\mathbf{k})}{U_{44}+U_{66}+(k_z^2B_z^2/4\pi\Phi_0)\Psi(\mathbf{k})}. \tag{20}$$

Equations (18-20) together with the condition that the current density along the c-axis should be smaller than the maximum current density j_c, determine completely the behavior of the PV lines and the JV. However, in further analysis it is convenient to investigate the dense ($\gamma s \gg a$) and dilute ($\gamma s \ll a$) pancake lattices separately.

II. JOSEPHSON VORTEX IN THE PRESENCE OF DENSE PV LATTICE

For the case of the dense PV lattice, many PV rows are placed on the nonlinear JV core (Fig. 1b, left sketch). It means that the magnetic field of a bare JV varies on scales larger than the distance between PV lines even near the JV core. Thus, the continuous approximation is applicable in the whole space. In this case $|k_y| < 1/\lambda_J < \pi/b$ and, therefore, the cosine and hyperbolic functions in (17) can be expanded in the series. Hence, the function Ψ can be rewritten as

$$\Psi = \frac{\Phi_0}{1+\lambda_{ab}^2k_z^2+\lambda_c^2k_y^2}. \tag{21}$$

Substituting this expression for Ψ into (19,20) and omitting the difference between $\mathbf{k}$ and $\mathbf{q}$, the equations for the dense PV lattice (which determine the field distribution and the energy of JV) are deduced as

$$\mathcal{B}_J = \int_{-1/\lambda_J}^{1/\lambda_J}\frac{dq_y}{2\pi}\int_{-1/s}^{1/s}\frac{dq_z}{2\pi} \times\frac{\Phi_0e^{iq_yy+iq_zz}}{1+\lambda_c^2q_y^2+\lambda_{ab}^2q_z^2+q_z^2B_z^2/(4\pi(U_{44}+C_{66}k_y^2))}, \tag{22}$$

and

$$\mathcal{E}_J = \frac{\Phi_0^2}{8\pi}\int_{-1/\lambda_J}^{1/\lambda_J}\frac{dq_y}{2\pi}\int_{-1/s}^{1/s}\frac{dq_z}{2\pi} \times\frac{1}{1+\lambda_c^2q_y^2+\lambda_{ab}^2q_z^2+B_z^2q_z^2/(4\pi(U_{44}+C_{66}q_y^2))}. \tag{23}$$

The last undefined parameter, λ_J, can be obtained from the condition $|\partial\mathcal{B}_J(y\approx\lambda_J, z=0)/\partial y| \sim (4\pi/c)j_c$:

$$\frac{\pi}{\lambda_c^2s} \simeq \lambda_J\int_{-1/\lambda_J}^{1/\lambda_J}dq_y\int_{-1/s}^{1/s}dq_z \times\frac{q_y^2}{1+\lambda_c^2q_y^2+\lambda_{ab}^2q_z^2+q_z^2B_z^2/(4\pi(U_{44}+C_{66}q_y^2))}. \tag{24}$$

The region of integration is shown in Fig. 2a. The rectangular domain of possible wave vectors replaces the usual elliptical one due to a peculiar core structure of JV. In anisotropic London model, the core of an ordinary vortex is defined by the elliptical stream line of the persistent current having the depairing value[18]. However, in our case the maximum value of q_z is determined by the layerness of the medium while the largest value of q_y is restricted by the Josephson critical current along the c-axis. The rectangular domain of wave vectors (Fig. 2 a) can be divided into "screened" ($|k_z| \gtrsim 1/b$) and "remote"($|k_z| < 1/b$) subdomains. The first one corresponds to the region where one can roughly neglect the weak logarithmical dependence on k_z in eq. (14) to express the tilt energy as:

$$U_{44} \approx \overline{U}_{44} + \overline{C}_{44}k_z^2, \tag{25}$$

with $\overline{U}_{44} = (B_z\Phi_0/32\pi^2\lambda_{ab}^4)\ln(1+\overline{k_z}^2/(\lambda_{ab}^{-2}+b^{-2}))$, $\overline{C}_{44} = \frac{B_z\Phi_0}{32\pi^2\lambda_c^2}\ln\left(\frac{\xi_{ab}^{-2}}{b^{-2}+(\overline{k_z}^2/\gamma^2)+\lambda_c^{-2}}\right)$ and $\overline{k_z} \sim \sqrt{1/bs}$.

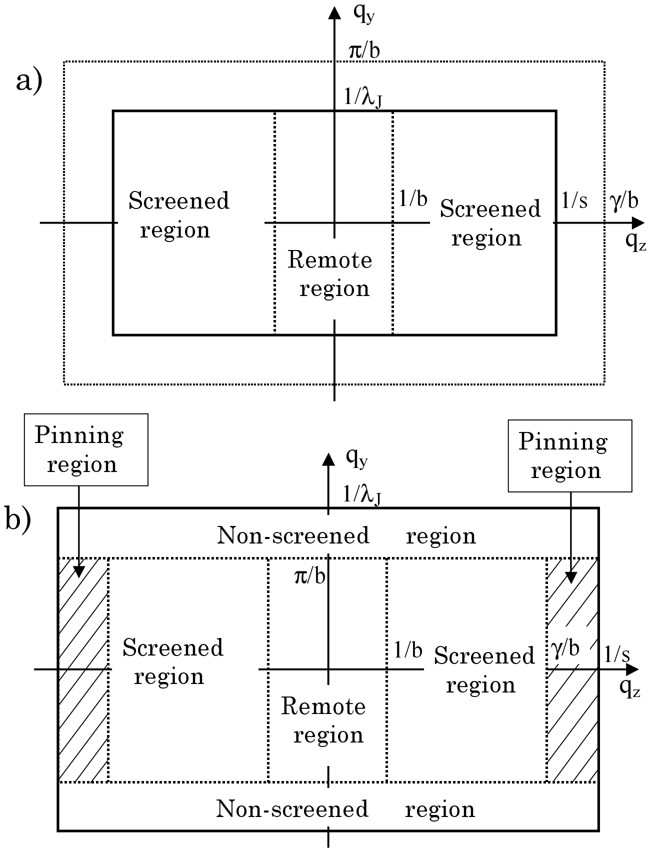

FIG. 2. The integration region in equations (19) and (20) for the dense PV lattice (a) and the dilute PV lattice (b). In the dense case (a), the region of the available wave vectors $\mathbf{k}$ of the PV lattice coincides with the accessible domain of wave vectors $\mathbf{q}$; the continuous approximation (21) for Ψ is always valid. The approximation (25) is correct in the "screened" domain of wave vectors, while it fails in the "remote" region. In the dilute case (b), the continuous approximation is correct only in the region $|q_y| \ll \pi/b$; $|q_z| \ll \gamma/b$; the "non-screened" region $|q_y| > \pi/b$ is not accessible for $\mathbf{k}$. The continuous approximation for $\Psi(\mathbf{k})$ is broken in the "pinning" region $|k_y| < \pi/b$; $\gamma/b \lesssim |k_z| \lesssim 1/s$.

The expression (25) is completely wrong in the "remote" region in which it is necessary to use equation (15). By using approximation (25) for the tilt energy, the integrals in equations (23) and (24) are easily evaluated (Appendix B) and we get

$$\lambda_J \approx \max\left(\frac{\lambda_c s}{\lambda_{ab}^{eff}}, \sqrt{\frac{\lambda_c s}{\lambda_{ab}^{eff}}\lambda_{ab}}\right) \qquad (26)$$

and

$$\mathcal{E}_J \approx \frac{\Phi_0^2}{16\pi^2\lambda_{ab}^{eff}\lambda_c}\left(\sqrt{\frac{C_{66}}{\overline{U}_{44}\lambda_{ab}^2}}\frac{\lambda_{ab}}{\lambda_J} + \ln\frac{\lambda_{cut}}{\lambda_J}\right), \qquad (27)$$

where $\lambda_{cut} \sim \min(\lambda_c, \min(\gamma b, \max(b\lambda_c/\lambda_{ab}^{eff}, \sqrt{b\lambda_c\lambda_{ab}/\lambda_{ab}^{eff}})))$, while the renormalized penetration depth λ_{ab}^{eff} is expressed as

$$\lambda_{ab}^{eff} = \sqrt{\lambda_{ab}^2 + \frac{B_z^2}{4\pi\overline{U}_{44}}}. \qquad (28)$$

The physical reason of the renormalization of the in-plane penetration depth is related to the screening of the JV field by currents born by the local inclination of PV lines. From eq. (26) it is easy to see that the size of the nonlinear JV core also decreases due to the interaction of JV and PVs. The similar conclusion was given earlier by Koshelev[7], who considered the additional phase variation of the order parameter born by the displacement of PVs. However, the shear contribution to the renormalization of $\mathcal{E}_J$ and λ_J was neglected in[7], which could be done only for $\lambda_J > \lambda_{ab}$ (see equations (26) and (27)). In the opposite case, *i.e.*, when the London penetration depth exceeds the JV core size, the shear deformation becomes relevant and, as a result, λ_J decreases with B_z slower than it was proposed in[7].

To understand how the field of JV is distributed in the real space, we rederive the results considering the free energy functional of the displacement u defined as a function of the spatial coordinates. In the limit $\gamma s \gg a$, the JV field varies on scales larger than the distance between PVs even near the JV core. This means that the field $\mathbf{h}_p$ along the x-axis can be averaged out on the scale larger than a:

$$h_p^* - \lambda_{ab}^2\frac{\partial^2 h_p^*}{\partial z^2} - \lambda_c^2\frac{\partial^2 h_p^*}{\partial y^2} = n^* = B_z\frac{\partial u}{\partial z}. \qquad (29)$$

However, the short range variations of the field $\mathbf{h}_p$ give the shear energy U_{66} and the tilt energy U_{44}. After ignoring the slow logarithmic dependence on $\mathbf{k}$ in the expression for U_{44}, one can conclude that the density of the tilt energy in the real space is $\overline{U}_{44}u^2(y,z)$, while the density of the shear energy is $U_{66} = C_{66}(\partial u/\partial y)^2$. Thus, the free energy functional is expressed as

$$F_{cross} = \frac{1}{8\pi}\int d^3\mathbf{R}\Bigg(4\pi C_{66}\left(\frac{\partial u}{\partial y}\right)^2 + 4\pi\overline{U}_{44}u^2 + \mathbf{h}_p^* B_z\frac{\partial \mathbf{u}}{\partial z} + 2\mathbf{h}_J\frac{\partial \mathbf{u}}{\partial z}\Bigg). \qquad (30)$$

The first three terms represent the elastic energy (born by shear, electromagnetic tilt and Josephson coupling tilt rigidity, respectively), but the last term is related to the interaction of the PV lines with the current generated by JV.

In order to get the complete set of equations for the displacement u and the averaged magnetic induction $\mathcal{B}_J$, we have minimized the functional (30) and have added together equations (3) and (29):

$$\begin{aligned} &-4\pi C_{66}\frac{\partial^2 u}{\partial y^2} + 4\pi \overline{U}_{44} u - 2B_z \frac{\partial \mathcal{B}_J}{\partial z} = 0, \\ &\mathcal{B}_J - \lambda_{ab}^2 \frac{\partial^2 \mathcal{B}_J}{\partial z^2} - \lambda_c^2 \frac{\partial^2 \mathcal{B}_J}{\partial y^2} = \Phi_0 \delta(y)\delta(z) + B_z \frac{\partial u}{\partial z}. \end{aligned} \tag{31}$$

This set of equations is applicable if the continuous approximation is valid ($\lambda_J \gg a$) and, strictly speaking, only when the tilt energy $U_{44}(k_z)$ can be replaced by the constant $\overline{U}_{44}$. The last condition fails on the distances far from JV ($z^2 + y^2/\gamma^2 > b^2$). In this "remote" region, the constant $\overline{U}_{44}$ has to be substituted by $-C_{44}^{eff}\partial^2/\partial z^2$. Besides, if $\lambda_{ab} > \gamma s$, the parameter $\overline{U}_{44}$ should be replaced by $-\overline{C}_{44}\partial^2/\partial z^2$ near the JV core ($z < \lambda_{ab}/\gamma$).

Even though we consider only the situation when the set of equation (31) is valid, *i.e.*, the case $\lambda_{ab} < \gamma s$ and the region $z^2 + y^2/\gamma^2 < b^2$, the solution of equations (31) seems to be quite complicated. The relation between the displacement u and the magnetic induction $\mathcal{B}_J$, which is obtained from the first equation of (31), becomes nonlocal due to the shear rigidity of the PV lattice:

$$u = \frac{B_z}{8\pi\sqrt{C_{66}\overline{U}_{44}}} \int_{-\infty}^{\infty} d\tilde{y} \frac{\partial \mathcal{B}_J(\tilde{y}, z)}{\partial z}\, e^{-|y-\tilde{y}|/\delta} \tag{32}$$

where $\delta = \lambda_{ab}\sqrt{C_{66}/(\overline{U}_{44}\lambda_{ab}^2)} \sim \lambda_{ab}$ is the characteristic length of a nonlocality. However, the nonlocality is irrelevant if the space scale of the variation of $\mathcal{B}_J$ is substantially large then δ, *i.e.*, if $\lambda_J \gg \lambda_{ab}$. In such a case, the equations (31) for $\mathcal{B}_J$ and u can be decoupled

$$\begin{aligned} &u = \frac{B_z}{4\pi U_{44}} \frac{\partial \mathcal{B}_J}{\partial z}, \\ &\mathcal{B}_J - (\lambda_{ab}^{eff})^2 \frac{\partial^2 \mathcal{B}_J}{\partial z^2} - \lambda_c^2 \frac{\partial^2 \mathcal{B}_J}{\partial y^2} = \Phi_0 \delta(y)\delta(z). \end{aligned} \tag{33}$$

The equation (33) for induction $\mathcal{B}_J$ is the London equation with the renormalized in-plane penetration depth λ_{ab}^{eff}. Therefore, the field distribution $\mathcal{B}_J$, not far from the center of the Josephson vortex ($z^2 + y^2/\gamma^2 \lesssim b^2$), can be approximated as

$$\mathcal{B}_J = \frac{\Phi_0}{2\pi\lambda_{ab}^{eff}\lambda_c} \mathrm{K}_0\left(\sqrt{z^2/(\lambda_{ab}^{eff})^2 + y^2/\lambda_c^2}\right), \tag{34}$$

where $\mathrm{K}_0(x)$ is a modified Bessel function of zero order. Using the free energy functional (30) and equations (31), it is easy to show that the energy of JV is determined by the field in its center, *i.e.*, $\mathcal{E}_J = \Phi_0/(8\pi)\mathcal{B}_J(y \approx \lambda_J, z \approx s)$:

$$\mathcal{E}_J = \frac{\Phi_0^2}{16\pi^2 \lambda_{ab}^{eff}\lambda_c} \ln(\lambda_{ab}^*/s) \tag{35}$$

with the length $\lambda_{ab}^* = \lambda_{ab}^{eff}$. However, the set of equations (31) becomes incorrect in the region $z^2 + y^2/\gamma^2 > b^2$ which cuts off that length as $\lambda_{ab}^* \approx b$. Thus, the expression (35) coincides with the earlier obtained equation (27) in the studied case $\lambda_J > \lambda_{ab}$. The results (34,35) can be interpreted in terms of the effective anisotropy parameter $\gamma^{eff} = \lambda_c/\lambda_{ab}^{eff}$ which governs the JV lattice. Since $\lambda_{ab}^{eff} > \lambda_{ab}$, the effective anisotropy γ^{eff} is reduced in the presence of PVs with respect to the "bare" one $\gamma = \lambda_c/\lambda_{ab}$. The similar anisotropy γ^{eff} was earlier introduced[7] as a ratio $\gamma^{eff} = \lambda_J/s$, but these two different definitions of γ^{eff} give the same value in the case $\lambda_J > \lambda_{ab}$ when the shear deformation is irrelevant.

Here, we discuss how the core size and the JV energy are changed with the magnetic induction B_z if $\gamma s > \lambda_{ab}$. For quite high magnetic inductions $B_z \gtrsim B_1 = (\Phi_0/\lambda_{ab}^2) \times (\gamma s/\lambda_{ab})^2$, the size of the nonlinear core λ_J is smaller than λ_{ab} and the shear contribution to the free energy is important. The second logarithmic term in the JV energy (27) can be omitted, and the core size obeys the equation $\lambda_J(B_z) \simeq \sqrt{\gamma s a}$. With decreasing of induction, the core size increases proportionally to $B_z^{-1/4}$ and reaches λ_{ab} at $B_z \approx B_1$. At low fields, the shear interaction between rows is irrelevant, the JV core size becomes $\lambda_J = \lambda_c s/\lambda_{ab}^{eff} \approx \gamma s a/\lambda_{ab}$, and the energy of JV is determined by the logarithmic term in (27). Below the field Φ_0/λ_{ab}^2, at which the distance a between PVs exceeds λ_{ab}, the currents generated by PVs practically do not influence on the JV field and, thus, the renormalization of λ_{ab}, λ_J and the $\mathcal{E}_J$ vanishes. In the case of $\lambda_{ab} > \gamma s$ the physical picture is different from the previous situation. The core size obeys the law $\lambda_J \simeq \sqrt{\gamma s a}$ at fields $B_z > \Phi_0/(\gamma s)^2$. Below this field, the effective value of the in-plane London penetration depth $\lambda_{ab}^{eff} \sim \lambda_{ab}^2/a$ (28) is still larger than λ_{ab}, while the JV core size is saturated as $\lambda_J = \gamma s$. This means that JV field shows different behavior far from JV ($z^2 + y^2/\gamma^2 > b^2/\gamma^2$), where the redistribution due to the local inclination of PV lines is still important, and close to the JV core.

III. JOSEPHSON VORTEX IN THE PRESENCE OF DILUTE PV LATTICE.

Far from the JV center, $z^2 + y^2/\gamma^2 > b^2/\gamma^2$, the JV field varies slowly which causes the smooth variation of the displacement u even for the case of the dilute PV lattice ($a > \gamma s$). In that spatial region, the continuous approximation is still valid. On the other hand, near the JV core ($|y| < b$), the JV current increases quite fast inducing a large displacement of the PV stack placed on the center of JV. In this case, the continuous approximation is not applicable. To describe such physical situation, we consider the wave vector area of $\mathbf{k}$ divided into two domains (Fig. 2b). In the first interval $|k_y| < \pi/b$ and $|k_z| < \gamma/b$, the function Ψ can be still roughly approximated by equation

$\Psi \approx \Phi_0/(1+\lambda_c^2 k_y^2+\lambda_{ab}^2 k_z^2)$, while $\Psi \approx \Phi_0 b/(2\lambda_c\lambda_{ab}k_z)$ in the second region $|k_y| < \pi/b$ and $\gamma/b < |k_z| < 1/s$ ("pinning" region in Fig. 2b). Following this approach, the energy of JV is evaluated as

$$\begin{aligned}\mathcal{E}_J(a \gg \gamma s) \approx {} & \frac{\Phi_0^2}{8\pi}\int_{-\pi/b}^{\pi/b}\frac{dq_y}{2\pi}\int_{-\gamma/b}^{\gamma/b}\frac{dq_z}{2\pi} \\ & \times \frac{1}{1+\lambda_c^2 q_y^2+\lambda_{ab}^2 q_z^2+B_z^2 q_z^2/(4\pi(U_{44}+U_{66}))} \\ & + \frac{\Phi_0^2}{16\pi^2\lambda_c\lambda_{ab}}\ln\left(\frac{b}{\gamma s}\right) \\ & - \frac{B_z\Phi_0^3}{128\pi^3 a\lambda_c^2\lambda_{ab}^2}\int_{\gamma/b}^{1/s}\frac{dk_z}{U_{44}+B_z\Phi_0 k_z/(8\pi\lambda_c\lambda_{ab}a)}. \end{aligned} \tag{36}$$

The first term comes from the spatial region far from the center of JV while the second and the third terms are related to the vicinity of the JV center. The screening of the "bare" JV field vanishes near JV ("non-screened" region in **k**-space) which determines the second term in (36). The last term in (36) represents the energy gain due to the strong interaction between the PV line placed on the JV core and the JV currents (the energy gain of a PV stack placed on a JV in the limit $\gamma s \gg \lambda_{ab}$ and $B_z \to 0$ was calculated by Koshelev[7]). Since the last term is sensitive to the mutual position of JV and the nearest PV line, this contribution can be called as the "crossing lattice pinning". Using the results of Appendix B and taking into account that the evaluation $B_z\Phi_0 k_z/(8\lambda_c\lambda_{ab}a) \lesssim \overline{C}_{44}k_z^2$ is held in the "pinning region" ($k_z > \gamma/b$), the energy of JV is finally obtained:

$$\begin{aligned}\mathcal{E}_J \approx {} & \frac{\Phi_0^2}{16\pi^2\lambda_c\lambda_{ab}^{eff}}\left(\frac{2\mu_1\overline{C}_{44}\gamma^2}{\pi\overline{U}_{44}\lambda_{ab}^2}\frac{\lambda_{ab}^3}{b^2\lambda_{ab}^{eff}}+\sqrt{\frac{\mu_2^2 C_{66}}{\overline{U}_{44}\lambda_{ab}^2}}\frac{\lambda_{ab}}{b}\right) \\ & + \frac{\Phi_0^2}{16\pi^2\lambda_c\lambda_{ab}^{eff}}\ln\left(\frac{\lambda_{cut}}{b}\right)+\frac{\phi_0^2}{16\pi^2\lambda_c\lambda_{ab}}\ln\left(\frac{b}{\gamma s}\right) \\ & - \mu\frac{\Phi_0^2}{4\pi a\lambda_c}\arctan\left(\frac{b-\gamma s}{\sqrt{\overline{U}_{44}/\overline{C}_{44}}sb+\gamma\sqrt{\overline{C}_{44}/\overline{U}_{44}}}\right), \end{aligned} \tag{37}$$

where $\mu = B_z\Phi_0/(32\pi^2\lambda_c\lambda_{ab}^2\sqrt{\overline{C}_{44}\overline{U}_{44}}) < 1$ is the dimensionless function depending quite slowly on B_z and the numerical parameters μ_1 and μ_2 are about unity.

Next, we will discuss how the renormalization of the JV energy comes in with increasing of the z-component of the magnetic field. At low fields, $B_z \ll \Phi_0/\lambda_{ab}^2$ ($a \gg \lambda_{ab}$), the first term and the last term in (37) can be omitted and the expression for the energy of a "bare" JV reported earlier in[19,20] is reproduced

$$\mathcal{E}_J = \frac{\Phi_0^2}{16\pi^2\lambda_c\lambda_{ab}}\ln\left(\frac{\lambda_c}{\gamma s}\right). \tag{38}$$

For the case $\lambda_{ab} > \gamma s$, the renormalization of JV energy becomes relevant at $B_z \approx \Phi_0/\lambda_{ab}^2$, *i.e.*, earlier than the JV core size starts to decrease which occurs only in fields $B_z > \Phi_0/(\gamma s)^2$. The origin of this behavior is that the additional current along the c-axis induced by tilted PV stacks is much smaller than j_c near JV core in the field interval $\Phi_0/\lambda_{ab}^2 \lesssim B_z \lesssim \Phi_0/(\gamma s)^2$, but the inclination of all PV lines can still cause the renormalization of the JV field on scales larger than a. In the field interval $\Phi_0/\lambda_{ab}^2 < B_z \lesssim \Phi_0/\gamma^2 s^2$, the main contribution to the Josephson vortex energy (37) comes from the first term related to the tilt elastic rigidity (born by Josephson coupling of PVs) and shear elasticity of the PV lattice. Strictly speaking, from our rough estimation of (20), we can not conclude how strongly $\mathcal{E}_J$ is suppressed in that field interval, *i.e.* in the presence of the dilute PV lattice. Nevertheless, the pinning energy (last term in (37)) could be the same order of magnitude as the first and the second terms in (37) in fields $B_z \sim \Phi_0/\lambda_{ab}^2$ and may decrease $\mathcal{E}_J$ substantially.

Another interesting possibility arising due to the "crossing lattice pinning" is the rearrangement of the PV lattice in the presence of the JV sublattice. In the in-plane magnetic fields B_x, JVs form a triangular lattice with distances a_J and b_J between JVs (see inset in Fig. 3a). In general, the PV sublattice and the JV sublattice are not commensurate: $a_J \neq pb$ with integer p. This means that the considered one-component displacement of PVs $\mathbf{u} = (u(y,z),0,0)$ (the "shifted" PV lattice shown in Fig. 3a) does not provide the energy gain coming from the "crossing lattice pinning" since the PV rows can not occupy the centers of JVs. However, the PVs can be rearranged in order to occupy all JVs (the "trapped" PV lattice shown in Fig. 3b) if the PV lines shift also along the y-direction: $\mathbf{u} = (u_x(x,y,z),u_y(x,y,z),0)$. The "crossing lattice pinning" decreases the free energy of the "trapped" PV lattice, while the additional shear deformation acts in the opposite way through increasing the free energy. For the case $B_x < \gamma B_z$, the energy gain related to the "trapped" PV lattice is calculated by normalizing the last term of equation (37) per unit volume:

$$E_{tr} = \mu\frac{B_x\Phi_0}{4\pi a\lambda_c}\arctan\left(\frac{b-\gamma s}{\sqrt{\overline{U}_{44}/\overline{C}_{44}}sb+\gamma\sqrt{\overline{C}_{44}/\overline{U}_{44}}}\right). \tag{39}$$

But, in order to trap the PV lattice, the total displacement of PVs along the y-axis between the two nearest JV rows, *i.e.*, on the scale a_J, should be about b. Following the simple analysis[21], the extra shear deformation (inset in Fig. 3b) is about $\delta b/b \sim b/a_J$ (δb is the change of the distance between rows of PVs) and the energy loss E_{shear} can be estimated as:

$$E_{shear} \simeq \nu C_{66}\left(\frac{b}{a_J}\right)^2 \approx \nu C_{66}\frac{B_x}{\gamma B_z} \tag{40}$$

with numerical constant $\nu \lesssim 1$. For the case $\gamma s \gg \lambda_{ab}$, the shear elastic energy (40) is strongly suppressed in the fields $B_z < \Phi_0/(\gamma s)^2$ where the "crossing lattice pinning" is active, since C_{66} is exponentially small if $a > \lambda_{ab}$ (13).

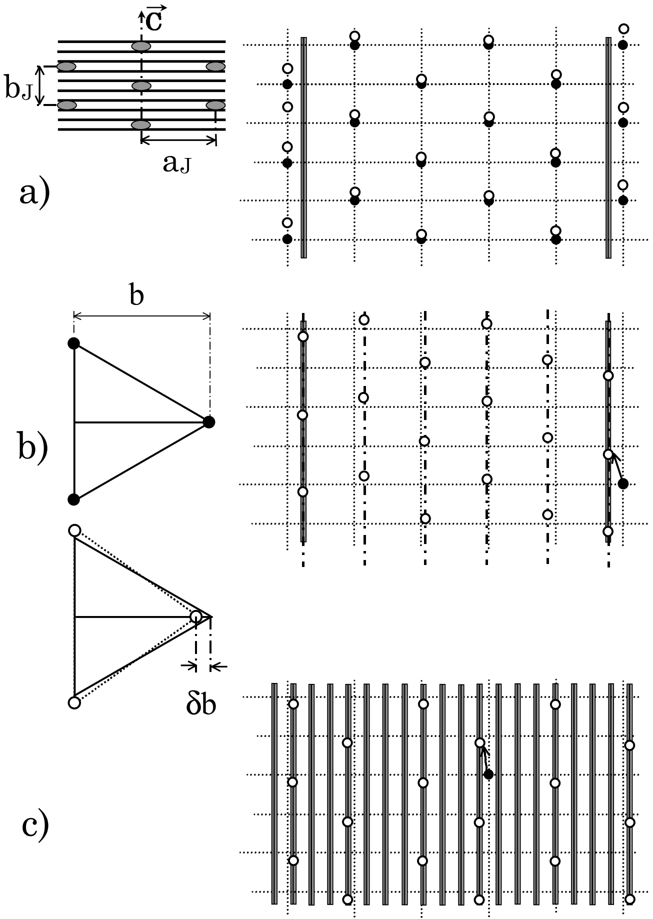

FIG. 3. The different substructures of the crossing lattice: a) the "shifted" PV lattice characterized by one-component displacement along JVs, b) the PV lattice trapped by the JV sublattice for the case when the distance a_J between JVs exceeds the distance b between PV rows, c) the "trapped" PV lattice for $a_J < b$, *i.e.*, in the case of the field orientations very close to the *ab*-plane. The dotted lines depict the rows of unperturbed lattice (crossings of these lines and filled circles mark the positions of unshifted PVs) in all sketches. Dashed-dotted lines indicate the rows of the "trapped" PV lattice which are deformed in order to match with JV sublattice. The arrows directed from the filled circles to the open ones show the two component displacement of PVs for the cases represented in sketches b) and c). Inset in a): the JV sublattice with lattice parameters a_J and b_J (lines mark the CuO$_2$ planes). Inset in b): the additional deformation of the PV lattice which is required for trapping of PVs by JVs. The upper sketch is the equilateral triangle of the unperturbed PV lattice which is incommensurate with JV lattice ($a_J \neq pb$ with integer p). The lower sketch is the isosceles triangle of the PV lattice matched with the JV sublattice ($a_J = p(b + \delta b)$).

Therefore, the "trapped" PV lattice seems to be realized as soon as $a > \gamma s$. In the opposite case, $\lambda_{ab} \gtrsim \gamma s$, the transformation[22] from the "shifted" PV lattice to the "trapped" PV lattice occurs when the energy gain E_{tr} exceeds the energy loss E_{shear}. It happens in a certain out-of-plane field between the field $\Phi_0/(\gamma s)^2$, at which the "crossing lattice pinning" is activated, and the field $B_z \sim \Phi_0/\lambda_{ab}^2$, where the shear elastic energy rapidly decreases. Next, we discuss the difference between the considered "trapped" state and the "chain" state proposed for the crossing lattice[7]. The "trapped" state is related to the rearrangement of PVs on the scale a_J between the nearest rows of JVs. On the other hand, the "chain" state is associated with the creation of an extra PV row (an interstitial in the PV lattice) on a JV, but the influence of the neighbouring JVs is completely ignored. As a result, the "trapped" and "chain" states have the different in-plane field dependence of the out-of-plane transition fields. The out-of-plane transition field[23] between the "shifted" and "trapped" PV lattices does not depend on H_{ab} in contrast to the H_{ab}-dependent out-of-plane field[7] of the destruction of the "chain" state. Since the analysis[7] is correct only in the case of $\gamma s \gg \lambda_{ab}$ and $a \gg \lambda_{ab}$, the transformation of the PV lattice discussed here seems to be more likely in the case $\lambda_{ab} > \gamma s$.

IV. PHASE DIAGRAM OF VORTEX LATTICE IN TILTED MAGNETIC FIELDS

In this section we discuss the vortex lattice structures formed at different field orientations. The tilted lattice consists of mono-oriented vortices and transforms continuously from the tilted PV stacks in fields near the *c*-axis (Fig. 4a) to the long JV strings connected by PV kinks for the field orientations close to the *ab*-plane (Fig. 4b). On the other hand, the tilted lattice is topologically different from the crossing vortex structure (Fig. 4c), and they replace each other via phase transition[6]. For the analysis of the vortex phase diagram in tilted fields, the free energy of the crossing and tilted vortex structures will be compared. We concentrate on the case $\gamma s < \lambda_{ab}$, when, according to Bulaevskii *et al.*[6] and Koshelev[20], the tilted lattice is energetically preferable above the lock-in transition[8]. We will consider a thin superconducting platelet with the *c*-axis perpendicular to the plate. In this geometry the lock-in transition occurs at very low fields[6] $B_z \approx (1 - n_z)\Phi_0/(4\pi\lambda_{ab}^2)\ln(\gamma s/\xi_{ab})$ with demagnetization factor n_z $(1 - n_z \ll 1)$.

For the field oriented close enough to the *c*-axis, $\tan\theta = B_x/B_z \ll \gamma$, the free energy of the tilted lattice F_t can be evaluated as $F_t = F_t^0 + \frac{1}{2}C_{44}^{tilt}(\mathbf{k} = 0)B_x^2/B_z^2$ in analogy to the analysis given in ref.[7]. Here, F_t^0 represents the free energy in the absence of the in-plane magnetic field, while the tilt modulus is expressed as $C_{44}^{tilt}(\mathbf{k} = 0) = B_z^2/4\pi + C_{44}^{eff}$ with C_{44}^{eff} defined in (15) for the case of $B_z \gtrsim \Phi_0/(4\pi\lambda_{ab}^2)$. As a result, we have:

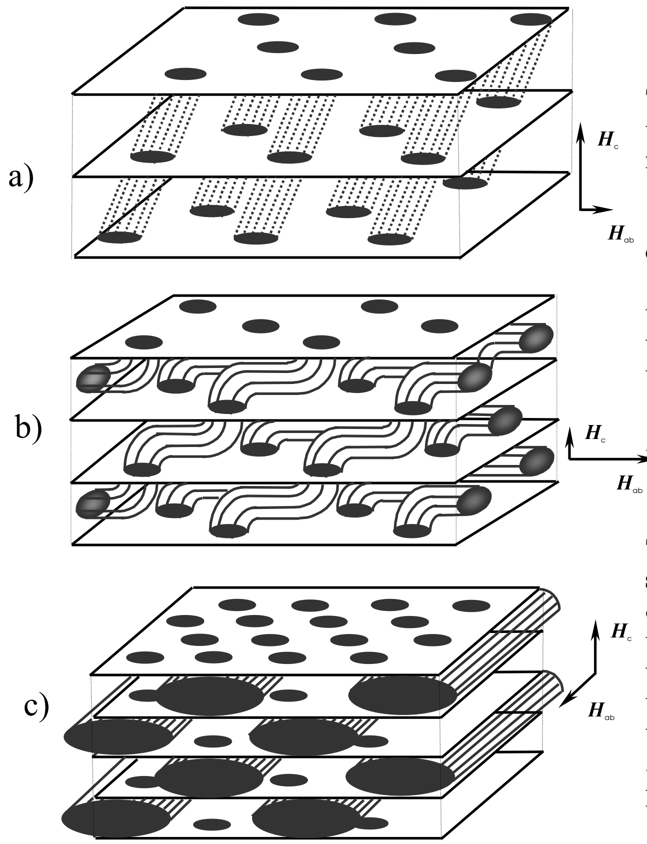

FIG. 4. The 3D sketches of the different vortex structures in the tilted magnetic field with the components H_c and H_{ab} along the c-axis and in the ab-plane, respectively: a) the tilted vortex lattice near the c-axis (TI), when the current between CuO$_2$ planes is much smaller than the critical value j_c, *i. e.*, the Josephson strings linking PVs are not developed; b) the tilted vortex lattice far away from the c-axis (TII), when the JV strings are formed; c) the crossing vortex lattice.

$$F_t \simeq \frac{B_z^2}{8\pi} + \frac{\Phi_0 B_z}{32\pi^2\lambda_{ab}^2}\ln\frac{H_{c2\perp}}{B_z} + \frac{B_x^2}{8\pi} + 3.68\frac{\Phi_0^2}{2(4\pi\lambda_{ab})^4}\frac{B_x^2}{B_z^2} + \frac{B_x^2\Phi_0}{64\pi^2\lambda_c^2 B_z}\ln\frac{H_{c2\perp}}{B_z}, \qquad (41)$$

where $H_{c2\perp} = \Phi_0/2\pi\xi_{ab}^2$. The first two terms form the free energy for $B_x = 0$. The third term is the in-plane magnetic energy, the fourth one comes from the electromagnetic interaction of the inclined PVs, and the last contribution is connected with the Josephson coupling of PVs.

The free energy of the crossing lattice F_c consists of two contributions from the PV sublattice and the JV sublattice while the interaction of PVs and JVs is taken into account through the renormalization of the JV energy:

$$F_c \simeq \frac{B_z^2}{8\pi} + \frac{\Phi_0 B_z}{32\pi^2\lambda_{ab}^2}\ln\frac{H_{c2\perp}}{B_z} + \frac{B_x^2}{8\pi} + \frac{B_x}{\Phi_0}\mathcal{E}_J. \qquad (42)$$

The renormalized JV energy, $\mathcal{E}_J$, is defined by equation (20) in which the lower limits of integrations are restricted by the conditions $q_y,\ k_y \gtrsim 1/a_J$ and $q_z,\ k_z \gtrsim 1/b_J$.

The tilted lattice is energetically preferable in the fields oriented near the c-axis because $F_t \propto B_x^2$, while $F_c \propto B_x$, *i. e.*, $F_t < F_c$ for low B_x. The phase boundary between the tilted lattice and the crossing structure can be obtained from the condition $F_t = F_c$ which is rewritten in the form:

$$B_x \simeq \frac{\mathcal{E}_J}{\Phi_0}\frac{B_z^2}{1.84\Phi_0^2/(4\pi\lambda_{ab})^4 + \Phi_0 B_z/(64\pi^2\lambda_c^2)\ln(H_{c2\perp}/B_z)}. \qquad (43)$$

The transition from the tilted lattice to the crossing structure occurs at the field oriented quite close to the c-axis for high anisotropic superconductors due to: 1) the high energy cost of the inclination of PV stacks in the tilted lattice related to the electromagnetic interaction of PVs, and 2) the decrease of the JV energy in the crossing lattice structure. For the dense PV lattice $B_z \gg \Phi_0/(\gamma s)^2$ and $\lambda_{ab} > \gamma s$, equation (43) can be simplified:

$$B_x \simeq \sqrt{\frac{C_{66}}{\overline{\overline{U}}_{44}\lambda_{ab}^2}}\,\frac{2\lambda_{ab}^2}{\lambda_J\lambda_{ab}^{eff}}\,\frac{B_z^2}{\frac{\gamma\Phi_0}{4.3\pi^2\lambda_{ab}^2} + \frac{B_z}{2\gamma}\ln(H_{c2\perp}/B_z)}. \qquad (44)$$

Next, we will study the field orientations close to the ab-plane, $B_x > \gamma B_z$. Here, the electromagnetic interaction between PVs in the tilted lattice is not so important and the free energy in the low c-axis fields $B_z < \Phi_0/\lambda_{ab}^2$ is reduced[6] to:

$$F_t \simeq \frac{B_x^2}{8\pi} + \frac{\Phi_0 B_x}{32\pi^2\lambda_{ab}\lambda_c}\ln\frac{\Phi_0}{\gamma s^2 B_x} + \frac{H_J B_z}{4\pi}, \qquad (45)$$

where $H_J = \Phi_0/(4\pi\lambda_{ab}^2)\ln(\gamma s/\xi_{ab})$. The first two terms are related to the energy of JV strings while the last one is associated with the energy cost of the formation of PV kinks. In more detail, the PV kink generates the in-plane current which decreases with the distance r from the kink center as $1/r$ up to a critical radius r_0 of the region with 2D behavior where the current along the c-axis is about the maximum possible current j_c[6]. At larger distances, the in-plane current decays exponentially. Simple evaluation gives $r_0 = \gamma s$ for the PV kink[6]. We note, that the tilted vortex lattice in the considered angular range of the magnetic field orientations seems to exist as a kink-walls substructure, where kinks (belonging to different vortices) are collected in separated walls parallel to the yz-plane[20]. For the kink-wall substructure of the tilted lattice, the contribution to the free energy (45), attributed to the PV kinks, is slightly reduced in the high in-plane magnetic fields $B_x > \Phi_0/\gamma s^2$[20], which can be taken into account through renormalization $H_J = \Phi_0/(8\pi\lambda_{ab}^2)\ln(\gamma H_{c2}/B_x)$.

In the considered field interval, $B_x > \gamma B_z$, $B_z \ll \Phi_0/\lambda_{ab}^2$, the renormalization of the JV energy in the crossing lattice structure vanishes. However, the interaction of PV and JV sublattices still manifests itself through the "crossing lattice pinning":

$$F_c = \frac{B_x^2}{8\pi} + \frac{\Phi_0 B_x}{32\pi^2\lambda_{ab}\lambda_c}\ln\frac{\Phi_0}{\gamma s^2 B_x} + \frac{H_{c1\perp}B_z}{4\pi}$$
$$-\mu B_z\sqrt{\frac{B_x\Phi_0}{16\pi^2\gamma\lambda_{ab}^2}}\arctan\left(\frac{1-\sqrt{B_x/H_0}}{\sqrt{H_\lambda^x/H_0}+\sqrt{B_x/H_\lambda^x}}\right), \quad (46)$$

with $H_{c1\perp} = \Phi_0/(4\pi\lambda_{ab}^2)\ln(\lambda_{ab}/\xi_{ab})$ (the critical radius r_0 for the in-plane currents of a PV stack is about λ_{ab}[6]), $H_0 = \Phi_0/\gamma s^2$ and $H_\lambda^x = \gamma\Phi_0/\lambda_{ab}^2$. The third term is the energy of the unperturbed PV lattice, while the last term corresponds to the "crossing lattice pinning" contribution which can significantly decrease the free energy F_c in the in-plane field interval $\gamma\Phi_0/\lambda_{ab}^2 \lesssim B_x \lesssim \Phi_0/\gamma s^2$. The difference between the "crossing lattice pinning" contributions to the free energy in the cases of low $B_x < \gamma B_z$ and high $B_x > \gamma B_z$ in-plane fields (see equations (39), (46)), emerges because the number of PV lines is sufficient to occupy all JVs (Fig. 3b) at $B_x < \gamma B_z$ while some JV strings do not carry PV rows (Fig. 3c) in the opposite case. By analyzing equations (45) and (46), we can conclude that, at least for $B_x \lesssim \gamma\Phi_0/\lambda_{ab}^2$ and $B_x \gtrsim \Phi_0/\gamma s^2$, the tilted lattice exists near the ab-plane since the condition $F_t < F_c$ is held due to the inequality $H_J < H_{c1\perp}$. The tilted lattice is replaced by the crossing lattice with increasing the out-of-plane magnetic field above $B_z = B_x/\gamma$. However, it is difficult to determine the contour of the possible phase line between the crossing and tilted vortex structures, since it requires the more precise calculations of the free energies F_c and F_t in the region $B_x < \gamma B_z$. In the intermediate in-plane magnetic fields $\gamma\Phi_0/\lambda_{ab}^2 \lesssim B_x \lesssim \Phi_0/\gamma s^2$, the "crossing lattice pinning" could make the crossing structure to be more energetically preferable with respect to the tilted lattice. In that case, the crossing lattice (CII, Fig. 3b) with $a < a_J$ transforms into the crossing lattice (CIII, Fig. 3c) with the extremely dilute PV sublattice $a > a_J$ at the angle $\theta = \arctan B_x/B_z \sim \arctan\gamma$.

Therefore, we find a complicated picture of phase transitions between the tilted vortex structure and the crossing vortex structure in the case $\gamma s < \lambda_{ab}$. The proposed phase diagram[24] is shown in figure 5. As it was suggested earlier[7] and according to our calculations by using equation (43), the tilted vortex structure (TI) of inclined PV stacks (see Fig. 4a) can be replaced by the crossing lattice quite close to the c-axis (see phase diagram obtained for $\gamma = 500$, inset in Fig. 5).

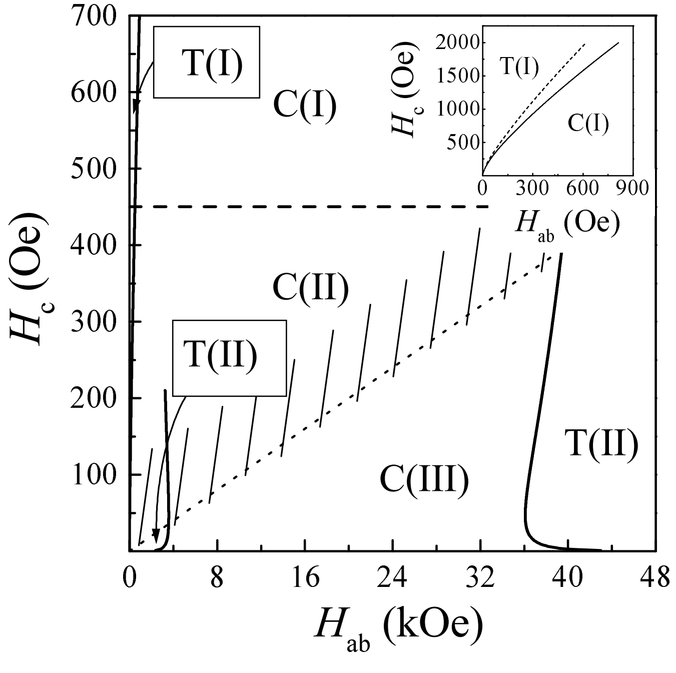

FIG. 5. The proposed phase diagram of the vortex solid phase in the oblique magnetic fields calculated using equations (39), (40), (43), (45) and (46) with parameters mentioned in the text, $T = 45$ K, $\gamma = 100$ and $\nu = 1$. The dotted line is the line $B_x = \gamma B_z$, while the shaded area marks the region inside which the transition from the crossing lattice C(II) to the tilted lattice T(II) or the crossing lattice C(III) happens. The arrows from enframed TI and TII are directed toward the regions where these vortex structures are realized. Inset: the part of the phase diagram close to the c-axis for strongly anisotropic superconductors with $\gamma = 500$ ($\gamma s > \lambda_{ab}$) and $T = 45$ K; the solid line marking the transition from the tilted lattice (TI) to the crossing lattice is obtained from eq. (43), while the dashed line, corresponding to the same transition, is calculated by using eq. (6) of Ref.[7]. The parameters are chosen to give some insight to the behavior of $Bi_2Sr_2CaCu_2O_{8-\delta}$ in the oblique magnetic fields.

Nevertheless, in the high c-axis magnetic fields, the calculated in-plane magnetic fields of this transition are higher than ones obtained by using the model[7]. This difference comes from the shear contribution to $\mathcal{E}_J$ which was omitted in ref.[7]. The crossing lattice, which exists in a wide angular range, can have different substructures. At high enough out-of-plane fields $B_z > \Phi_0/\gamma^2 s^2$, the "shifted" PV sublattice is realized in the crossing lattice structure (CI, Fig. 3a). In this substructure, the JV currents shift the PVs mostly along the x-axis. The "shifted" phase can transform into the "trapped" PV lattice (CII, Fig. 3b), when the energy gain related to the "crossing lattice pinning" exceeds the energy needed for the additional shear deformation (the dashed line in Fig. 5 separating CI and CII has been obtained from the condition $E_{tr} = E_{shear}$). Around the line $B_x = \gamma B_z$, the lattice CII can be changed by the tilted lattice (TII) with JV strings linked by PV kinks (Fig. 4b) or by the crossing lattice structure (CIII, Fig. 3c) at which all PV stacks are placed on a few JVs. The domain in the $H_c - H_{ab}$ phase diagram with the lattice CIII is determined by the condition $F_c < F_t$ where F_t and F_c are defined by the equations (45) and (46), respectively. With increasing temperature, the region of the lattice CIII becomes narrower and disappears at a certain temperature (see Fig. 6). The proposed phase diagram suggests the possibility of the re-entrant tilted-crossing-tilted phase transition as the magnetic field (at least with low $B \lesssim \gamma\Phi_0/\lambda_{ab}^2$ or high $B \gtrsim \Phi_0/\gamma s^2$ absolute value) is tilted away from the c-axis to the ab-plane. Such possibility for low fields was earlier mentioned in the works[11,13] in which the interaction of crossed sublattices was not considered. Moreover, we note that the instability of the tilted lattice was found numerically by Thompson and Moore[25] (for $\gamma \lesssim 100$) only at the intermediate field orientations $0^\circ < \theta_1 < \theta < \theta_2 < 90^\circ$, which could also support the discussed scenario. The parameters taken for the $H_c - H_{ab}$ phase diagram at $T = 45$ K (Fig. 5) and the $H_{ab} - T$ phase diagram at the magnetic field orientation $B_z = B_x/\gamma$ (Fig. 6) were chosen to give some insight into the behavior of vortex array in BSCCO in the tilted magnetic fields (see further discussion) as $\lambda_{ab} = 2000/\sqrt{1 - T^2/T_c^2}$ Å, $\xi_{ab} = 30/\sqrt{1 - T/T_c}$ Å, $s = 15$ Å, $T_c = 90$ K, $\gamma = 100$ ($\gamma = 500$ for inset in Fig.5 and $\gamma = 150$ for inset in Fig. 6).

V. CONCLUSION

This theoretical investigation was partially motivated by the recent intensive experimental studies of the vortex lattice melting transition[26–30] as well as transitions in the vortex solid phase[29,31] in $Bi_2Sr_2CaCu_2O_{8+\delta}$ single crystals. The observed linear decay of the c-axis melting field component H_c^{m} with in-plane fields[26,27] was interpreted[7] as an indication of the crossing vortex lattice. Thus, the tilted lattice could be replaced by the crossing vortex structure quite near the c-axis. According to our calculations, the angle where such transition may occur is about 7° at $B_z \approx 100$ Oe and $\gamma \approx 500$ while that angle reaches 14.5° in the higher out-of-plane field $B_z = 500$ Oe, which correlates well with the disappearance of the hexagonal order along the c-axis found by neutron measurements[32]. With further tilting of the magnetic field, the linear dependence of the c-axis melting field component $H_c^{\mathrm{m}}(H_{ab})$ abruptly transforms into a weak dependence[27–29], which, as was shown[28], can not be explained in the frame of the model[7]. Such behavior suggests a phase transition in the vortex solid phase in tilted magnetic fields in $Bi_2Sr_2CaCu_2O_{8+\delta}$, which was detected in the recent ac magnetization measurements[29,31].

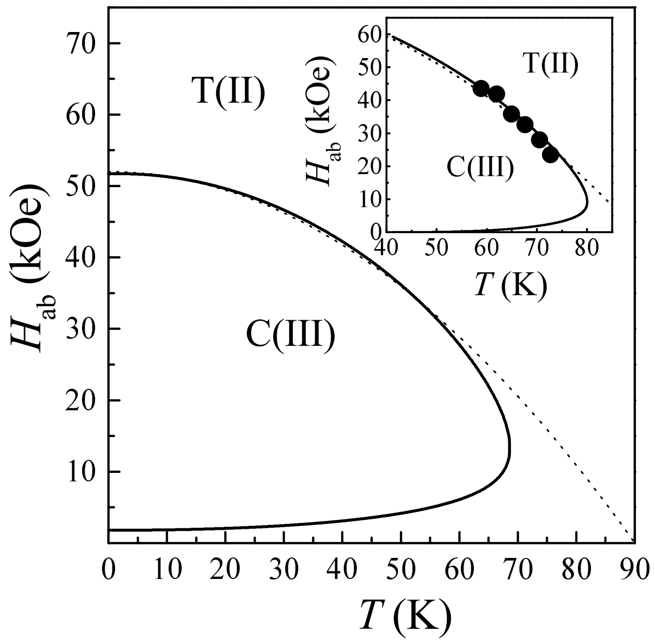

FIG. 6. The $H_{ab} - T$ phase diagram of the vortex solid phase at the field oriented near the ab-plane ($B_x/B_z = \gamma = 100$). The region of the crossing lattice phase (CIII) becomes narrower and finally disappears with increasing temperature. Inset: the same phase diagram for $\gamma = 150$. The dotted lines correspond to the experimentally found temperature dependence $H_{ab}^m \propto 1 - T^2/T_c^2$ of the in-plane characteristic fields of the vortex lattice melting transition in $Bi_2Sr_2CaCu_2O_{8+\delta}$ in the tilted fields[30] (for instance, symbols represented in the inset exhibit the temperature dependence of the maximum in-plane field of the vortex lattice melting transition).

As was mentioned by Ooi *et al.*[31], the behavior of the new anomaly of the local magnetization in BSCCO attributed to the phase transition in the vortex solid slightly reminds the peak effect related to the vortex pinning, which, in turn, could be induced by the vortex trapping by planar defects[21]. Such analogy, as well as a very weak dependence of the c-axis magnetic field component H_c^* of the novel phase transition on in-plane magnetic fields[31] in a wide angular range, could suggest the tansition from the "shifted" PV sublattice (CI) to the "trapped" PV sublattice (CII) in the crossing lattice structure. Our estimation of the c-axis field H_c^{trap} of the transition from CI to CII ($H_c^{trap} \approx 450$ Oe for $\gamma = 100$ at $T = 45$ K (see Fig. 5))[33] is in a reasonable agreement with experimental findings[31] $H_c^*(T = 45 \text{ K}) \approx 430$ Oe. Near the ab-plane, the properties of the observed anomaly changes abruptly and the field H_c^* sharply goes to zero[31], which may indicate a transformation[23] in the JV lattice or a trace of the phase transition from TII to CIII. At higher in-plane fields, the found step-wise behavior[28] of the vortex lattice melting transition may be related to the existence of one more phase transition in the solid phase. Interestingly enough, all characteristic in-plane fields of the vortex lattice melting transition depend on temperature[30] proportionally to $1 - T^2/T_c^2$, which is similar to the calculated temperature dependence of the phase transition from CIII to TII (see Fig. 6).

In summary, we discussed the crossing lattice structure in a strongly anisotropic layered superconductor in the framework of the extended anisotropic London theory. The renormalization of the JV energy in the crossing lattice structure was calculated in the cases of the dense PV lattice as well as the dilute PV lattice. It was shown, that the "crossing lattice pinning" can induce the rearrangement of the PV sublattice in the crossing lattice structure as soon as the out-of-plane magnetic field becomes lower than a certain critical value. The free energy analysis indicates a possibility of the re-entrant tilted-crossing-tilted lattice phase transition with inclination of the magnetic field away from the c-axis to the ab-plane in the case of $\lambda_{ab} > \gamma s$.

APPENDIX A. APPROXIMATE SUMMATION IN EQUATION (10)

Our aim is to sum the sequence:

$$\Phi_0 \sum_{n=-\infty}^{\infty} ik_z u(\mathbf{k}) \frac{f(k_z, k_y - 2\pi n/b) - (B_z/2\Phi_0) ik_z u(-\mathbf{k})}{1 + \lambda_{ab}^2 k_z^2 + \lambda_c^2 (k_y - 2\pi n/b)^2} = ik_z \Psi_1(k_y, k_z) u(\mathbf{k}) + (B_z/2\Phi_0) k_z^2 \Psi(k_y, k_z) u(\mathbf{k}) u(-\mathbf{k}). \quad \text{(A1)}$$

The equation (17) for $\Psi(k_y, k_z)$ can be directly obtained by using the well-known mathematical equality

$$\sum_n \frac{1}{r^2 + (t + 2\pi n/\alpha)^2} = \frac{\alpha}{2r} \frac{\sinh(r\alpha)}{\cosh(r\alpha) - \cos(t\alpha)}$$

with real numbers r, t, and α.

Next the sum $\Psi_1(k_y, k_z) = \Phi_0 \sum_{Q_y = 2\pi n/b} f(k_z, k_y - Q_y)/(1 + \lambda_{ab}^2 k_z^2 + \lambda_c^2 (k_y - Q_y)^2)$ needs to be estimated. By using inequailty $k_z \lesssim 1/s$, we obtain $f(k_z, k_y - Q_y) \approx f_J(k_y - Q_y)$ where $f_J \approx 1$ for $|k_y - Q_y| \lesssim 1/\lambda_J$ and zero otherwise. In the case of the dense PV lattice ($b \ll \lambda_J$) we retain only the term with $n = 0$ in the sum and get the expression $\Psi_1(k_y > 1/\lambda_J) = 0$ and $\Psi_1(k_y \lesssim 1/\lambda_J) = \Phi_0/(1 + \lambda_{ab}^2 k_z^2 + \lambda_c^2 k_y^2)$. Taking into account the inequality $k_y < 1/\lambda_J \ll 1/b$ and $\sqrt{1 + \lambda_{ab}^2 k_z^2}\, b/\lambda_c < b/(\gamma s) \ll 1$, one can rewrite $\Psi_1(k_y < 1/\lambda_J, b \ll \lambda_J) \simeq \Psi(k_y, k_z)$. Thus, we come to the equation (16).

For the case of the dilute PV lattice ($\lambda_J \ll b$), many terms give contributions to the sum $\Psi_1 \simeq \Phi_0 \sum_{n=-N}^{N} 1/(1 + \lambda_{ab}^2 k_z^2 + \lambda_c^2 (k_y - 2\pi n/b)^2)$, since inequality $|k_y - 2\pi n/b| < 1/\lambda_J$ is held until n exceeds $N \gg 1$. Thus, the function Ψ_1 is estimated as:

$$\Psi_1(k_y, k_z) \approx \Psi(k_y, k_z) - \frac{\Phi_0 b}{\pi} \int_{1/\lambda_J}^{\infty} \frac{dx}{1 + \lambda_{ab}^2 k_z^2 + \lambda_c^2 x^2} \quad \text{(A2)}$$

Finally, we obtain $\Psi_1 = (1 - \beta(k_y, k_z))\Psi$ with

$$\beta(k_y, k_z) \approx \frac{\cosh(\sqrt{1 + \lambda_{ab}^2 k_z^2}\, b/\lambda_c) - \cos(k_y b)}{\sinh(\sqrt{1 + \lambda_{ab}^2 k_z^2}\, b/\lambda_c)} \left(1 - \frac{2}{\pi} \arctan\left(\frac{\lambda_c}{\lambda_J \sqrt{1 + \lambda_{ab}^2 k_z^2}}\right)\right) \quad \text{(A3)}$$

At $|k_z| \ll 1/s$, it is easy to show that $\beta \lesssim \lambda_J/b \ll 1$ and the approximation $\Psi_1 = \Psi$ used in (16) is excellent. Only for $k_z \sim 1/s$, the function Ψ_1 can differ from the function Ψ by a factor about unity in the case of the dilute PV lattice (the factor is $1 - \beta \approx 0.5$ in the framework of our rough consideration). However, the correct estimation of the value of the factor depends on the type of the smoothing function and requires more precise analisys than one in the framework of the London approach. Therefore, we can always assume $\Psi_1 = \Psi$ in our semiquantitative consideration.

APPENDIX B. EVALUATION OF INTEGRALS IN EQUATIONS (23,24,36)

In this appendix, the integrals in equations (23,24,36) are evaluated. We start with the dense PV lattice, $a \ll \lambda_J$. In the region $q_z < 1/b$, the tilt energy is small (15). Therefore, the denominators of the integrands in (23,24) are substantially larger than ones in the case $q_z > 1/b$ and we can roughly neglect the contribution related to the region $q_z < 1/b$. Using equation (25) for the tilt energy in the domain $q_z > 1/b$, the integrals (23,24) can be rewritten as follows:

$$I = 2\int_{-1/\lambda_J}^{1/\lambda_J} dq_y \int_{1/b}^{1/s} dq_z \cdot \frac{f(q_y^2)}{1+\lambda_c^2 q_y^2+\lambda_{ab}^2 q_z^2 + B_z^2 q_z^2/(4\pi(\overline{U}_{44}+\overline{C}_{44}q_z^2+C_{66}q_y^2))}, \tag{B1}$$

where $f(q_y^2) = \Phi_0^2/32\pi^3$ for (23) and $f = \lambda_J q_y^2$ for (24). After multiplying numerator and denominator by factor of $\overline{U}_{44}+\overline{C}_{44}q_z^2+C_{66}q_y^2$, the expression (B1) is reduced to

$$I = 2\int_{-1/\lambda_J}^{1/\lambda_J} dq_y \int_{1/b}^{1/s} dq_z \cdot \frac{(\overline{U}_{44}+\overline{C}_{44}q_z^2+C_{66}q_y^2)f(q_y^2)}{(1+\lambda_c^2 q_y^2+\lambda_{ab}^2 q_z^2)(\overline{U}_{44}+C_{66}q_y^2)+\Big((1+\lambda_c^2 q_y^2+\lambda_{ab}^2 q_z^2)\overline{C}_{44}+\frac{B_z^2}{4\pi}\Big)q_z^2} \tag{B2}$$

The term $(1+\lambda_c^2 q_y^2+\lambda_{ab}^2 q_z^2)\overline{C}_{44}$ can be neglected with respect to $B_z^2/4\pi$ in the denominator. Indeed, the maximum value of $\lambda_c^2 q_y^2 \overline{C}_{44}$ (see eq. (25)) is about $\lambda_c^2 \overline{C}_{44} 1/\lambda_J^2 \sim B_z \Phi_0/\lambda_J^2 \ll B_z^2$, while the maximum value of $\lambda_{ab}^2 q_z^2 \overline{C}_{44}$ is $\lambda_c^2 \overline{C}_{44} 1/\lambda_J^2 \times (\lambda_J/\gamma s)^2$ which is even smaller, since $\lambda_J < \gamma s$ (see eq. (26)). Next, the integration in (B2) over q_z can be taken easily:

$$I = 4\int_{1/\lambda_c}^{1/\lambda_J} dq_y f(q_y^2)\Bigg(\frac{\overline{C}_{44}}{B_z^2/4\pi+\lambda_{ab}^2(\overline{U}_{44}+C_{66}q_y^2)}\frac{1}{s}+\frac{1}{\lambda_c q_y}\frac{\sqrt{\overline{U}_{44}+C_{66}q_y^2}\,\theta^*(q_y)}{\sqrt{B_z^2/4\pi+\lambda_{ab}^2(\overline{U}_{44}+C_{66}q_y^2)}}\Bigg) \tag{B3}$$

where the function θ^*, defined as

$$\theta^*(q_y) = \arctan\left(\frac{q_y^{-1}}{\gamma s}\sqrt{1+B_z^2/(4\pi\lambda_{ab}^2(\overline{U}_{44}+C_{66}q_y^2))}\right) - \arctan\left(\frac{q_y^{-1}}{\gamma b}\sqrt{1+B_z^2/(4\pi\lambda_{ab}^2(\overline{U}_{44}+C_{66}q_y^2))}\right),$$

determines the lower cutting value $1/\lambda_{cut}$ of q_y. Namely, by using (26) we can assume that the argument of the first arc tangent in the last expression is larger than 1, for most of values of q_y. Then, the value of $\theta^*(q_y)$ is about $\pi/2$ if the argument of the second arc tangent is smaller than 1; otherwise θ^* is close to zero. Thus, we obtain the expression for λ_{cut}:

$$\lambda_{cut} \approx \frac{b\gamma}{\sqrt{1+\frac{B_z^2}{4\pi\lambda_{ab}^2(\overline{U}_{44}+C_{66}\lambda_{cut}^{-2})}}} \approx \frac{\sqrt{2}b\gamma}{\left(1-\frac{b^2\gamma^2}{\delta^2}+\sqrt{\left(\frac{b^2\gamma^2}{\delta^2}-1\right)^2+4\frac{(\lambda_{ab}^{eff})^2 b^2\gamma^2}{\lambda_{ab}^2\delta^2}}\right)^{1/2}}$$

$$\sim \min(\lambda_c, \min(\gamma b, \max(b\lambda_c/\lambda_{ab}^{eff}, \sqrt{b\lambda_c\delta/\lambda_{ab}^{eff}}))),$$

where we denote $\delta = \sqrt{C_{66}/\overline{U}_{44}} \sim \lambda_{ab}$ and take into account that λ_{cut} should be smaller than λ_c. As a result, the integral (B3) can be evaluated as:

$$I = 4\int_{1/\lambda_c}^{1/\lambda_J} dq_y f(q_y^2)\frac{\overline{C}_{44}}{B_z^2/4\pi+\lambda_{ab}^2(\overline{U}_{44}+C_{66}q_y^2)}\frac{1}{s} + 2\pi\int_{1/\lambda_{cut}}^{1/\lambda_J} dq_y f(q_y^2)\frac{1}{\lambda_c q_y}\frac{\sqrt{\overline{U}_{44}+C_{66}q_y^2}}{\sqrt{B_z^2/4\pi+\lambda_{ab}^2(\overline{U}_{44}+C_{66}q_y^2)}}. \tag{B4}$$

In case of the dense PV lattice, the first integral is small and can be neglected. In addition, we also can omit the term $C_{66}q_y^2$ in the expression $B_z^2/4\pi+\lambda_{ab}^2 C_{66}q_y^2$. Finally, we have

$$I(a \ll \lambda_J) = 2\pi\frac{1}{\lambda_c\lambda_{ab}^{eff}}\int_{1/\lambda_{cut}}^{1/\lambda_J}\frac{f(q_y^2)dq_y}{q_y}\sqrt{1+\frac{C_{66}}{\overline{U}_{44}}q_y^2}. \tag{B5}$$

After taking $f(q_y^2) = \lambda_J q_y^2$ in (B5) and by ignoring $C_{66}q_y^2/\overline{U}_{44}$ in the case $\lambda_J > \lambda_{ab}$ or by neglecting unity in the opposite case, we obtain the expression $\lambda_J \approx \max\left(\frac{\lambda_c s}{\lambda_{ab}^{eff}}, \sqrt{\frac{\lambda_c s}{\lambda_{ab}^{eff}}\delta}\right)$. It coincides with (26) since $\delta \approx \lambda_{ab}$. The energy of JV (27) is easily derived if one puts $f(q_y^2) = \Phi_0^2/(32\pi^3)$ in (B5). Next, we roughly estimate the first integral in equation (36). The inequality $(1 + \lambda_c^2 q_y^2 + \lambda_{ab}^2 q_z^2)\overline{C}_{44} \ll B_z^2$ is still correct in the domain $q_z \ll \gamma/b$, $q_y \ll 1/b$ for $B_z \gg \Phi_0/\lambda_c^2$. Thus, we can get the estimation (B4) also for the dilute case ($a > \gamma s$). However, in contrary to the dense PV lattice, the contribution related to the first term in (B4) remains important:

$$I(a \gg \lambda_J) = 4\frac{\overline{C}_{44}\gamma}{\overline{U}_{44} b(\lambda_{ab}^{eff})^2}\int_{1/\lambda_c}^{\mu_1/b} dq_y f(q_y^2) + \frac{2\pi}{\lambda_c\lambda_{ab}^{eff}}\int_{1/\lambda_{cut}}^{\mu_2/b} dq_y \frac{f(q_y^2)}{q_y}\sqrt{1+\frac{C_{66}}{\overline{U}_{44}}q_y^2}. \quad \text{(B6)}$$

Here, we have introduced numerical parameters μ_1 and μ_2, since the upper limits of integration are not well defined. The corresponding contribution to the energy is obtained from the last equation for $f = \Phi_0^2/32\pi^3$ as presented in the text.

---

[*] On leave from All Russian Electrical Engineering Institute, 111250 Moscow, Russia

[+] On leave from Faculty of Sciences, University of Montenegro, PO Box 211, 81000 Podgorica, Montenegro, Yugoslavia

[1] G. Blatter, M. V. Feigel'man, V. B. Geshkenbein, A. I. Larkin, V. M. Vinokur, Rev. Mod. Phys. **66**, 1125 (1994).

[2] E. H. Brandt, Rep. Prog. Phys. **58**, 1465 (1995).

[3] A. I. Buzdin and D. Feinberg, J. Phys. (Paris) **51**, 1971 (1990); S. N. Artemenko and A. N. Kruglov, Phys. Lett. A **143**, 485 (1990); J. R. Clem, Phys. Rev. B **43**, 7837 (1991).

[4] L. Bulaevskii and J. Clem, Phys. Rev. B **44**, 10234 (1991).

[5] D. Feinberg, Physica **194C**, 126 (1992).

[6] L. N. Bulaevskii, M. Ledvij, and V. G. Kogan, Phys. Rev. B **46**, 366 (1992).

[7] A. E. Koshelev, Phys. Rev. Lett. **83**, 187 (1999).

[8] D. Feinberg and C. Villard, Phys. Rev. Lett. **65**, 919 (1990).

[9] A. Sudbo, E. H. Brandt, and D. A. Huse, Phys. Rev. Lett. **71**, 1451 (1993).

[10] L. L. Daemen, L. J. Campbell, A. Yu. Simonov, V. G. Kogan, Phys. Rew. Lett. **70**, 2948 (1993).

[11] G. Preosti and P. Muzikar, Phys. Rev. B **48**, 9921 (1993).

[12] W. E. Lawrence and S. Doniach, in Proceedings of 12th International Conference on Low Temperature Physics, Kyoto 1970, edited by E. Kanda (Keigaku, Tokyo, 1970), p. 361.

[13] M. Benkraouda and M. Ledvij, Phys. Rev. B **51**, 6123 (1995).

[14] D. A. Huse, Phys. Rev. B **46**, 8621 (1992).

[15] L. N. Bulaevskii, S. V. Meshkov, D. Feinberg, Phys. Rev. B **43**, 3728 (1991).

[16] E. H. Brandt, J. Low Temp. Phys. **26**, 735 (1977); the expression of C_{66} for $a_0 > \lambda_{ab}$ was presented, for instance, in G. Blatter, V. Geshkenbein, A. Larkin, H. Nordborg, Phys. Rev. B **54**, 72 (1996).

[17] A. E. Koshelev and P. H. Kes, Phys. Rev. B **48**, 6539 (1993).

[18] V. G. Kogan and L. J. Campbell, Phys. Rev. Lett. **62**, 1552 (1989).

[19] J. R. Clem, M. W. Coffey, and Z. Hao, Phys. Rev. B **44**, 2732 (1991).

[20] A. E. Koshelev, Phys. Rev. B **48**, 1180 (1993).

[21] I. F. Voloshin *et al.*, JETP **84**, 1177 (1997).

[22] One of the possible physical pictures of the replacement of the "shifted" PV lattice by the "trapped" PV lattice is the sequence of the phase transitions. At each of those transitions, the distance L between the nearest JV rows, occupied by PV rows, increases by a_J and takes values $L = a_J$ (lattice in Fig. 3b), $L = 2a_J$ (every second JV row is occupied), etc.

[23] The structural transitions between the Josephson vortex lattices with different periods[4], which are related to the layerness of the medium, cause the nonmonotonic dependence of a_J on the in-plane field[28]. Such behavior of the JV sublattice can induce the complicated alternation of the "shifted" and "trapped" states.

[24] For simplicity, we have assumed that the demagnetization factor n_z is very close to unity, *i.e.*, the lock-in transition and Meissner state are far below the considered region of B_z.

[25] A. M. Thompson and M. A. Moore, Phys. Rev. B **55**, 3856 (1997).

[26] S. Ooi, T. Shibauchi, N. Okuda, and T. Tamegai, Phys. Rev. Lett. **82**, 4308 (1999).

[27] J. Mirković, E. Sugahara, and K. Kadowaki, Physica **284B-288B**, 733 (2000).

[28] J. Mirković, S. E. Savel'ev, E. Sugahara, and K. Kadowaki, Phys. Rev. Lett. **86**, 886 (2001).

[29] M. Konczykowski, C. J. van der Beek, M. V. Indenbom, and E. Zeldov, Physica **341C-348C**, 1213 (2000).

[30] J. Mirkovic, S. Savel'ev, E. Sugahara, and K. Kadowaki, Meeting Abstracts of the Physical Society of Japan, vol. 55, issue 2, part 3, p. 504, 55th Annual Meeting, September 22-25, 2000; J. Mirkovic, S. Savel'ev, E. Sugahara, and K. Kadowaki, Physica **C**, to be published.

[31] S. Ooi, T. Shibauchi, K. Iteka, N. Okuda, T. Tamegai, Phys. Rev. B **63**, 20501(R) (2001).

[32] J. Suzuki, N. Metoki, S. Miyata, M. Watahiki, M. Tachiki, K. Kimura, N. Kataoka, and K. Kadowaki, Advances in Superconductivity XI, proc. of the 11th International Symposium on Superconductivity (ISS'98), November 16-19, 1998, Fukuoka, Japan, p. 553 (Springer Verlag).

[33] Note that the anisotropy parameter γ of BSCCO can change in quite wide range depending, in particular, on the oxygen stoichiometry (see for instance G. Balestrino *et al.,* Phys. Rev. B **51**, 9100 (1995)).